Cell Reports
Article

Oncogene Mimicry as a Mechanism of Primary Resistance to BRAF Inhibitors

Martin L. Sos,[1] Rebecca S. Levin,[1,2,5] John D. Gordan,[1,4,5] Juan A. Oses-Prieto,[2] James T. Webber,[3] Megan Salt,[4] Byron Hann,[4] Alma L. Burlingame,[2] Frank McCormick,[4] Sourav Bandyopadhyay,[3] and Kevan M. Shokat[1,*]
[1]Howard Hughes Medical Institute and Department of Cellular and Molecular Pharmacology, University of California, San Francisco, San Francisco, CA 94158, USA
[2]Department of Pharmaceutical Chemistry, University of California, San Francisco, San Francisco, California, CA 94158, USA
[3]Department of Bioengineering and Therapeutic Sciences, University of California, San Francisco, San Francisco, CA 94158, USA
[4]Department of Medicine, Helen Diller Family Comprehensive Cancer Center, University of California, San Francisco, San Francisco, CA 94143, USA
[5]These authors contributed equally to this work
*Correspondence: kevan.shokat@ucsf.edu
http://dx.doi.org/10.1016/j.celrep.2014.07.010

SUMMARY

Despite the development of potent RAF/mitogen-activated protein kinase (MAPK) pathway inhibitors, only a fraction of *BRAF*-mutant patients benefit from treatment with these drugs. Using a combined chemogenomics and chemoproteomics approach, we identify drug-induced RAS-RAF-MEK complex formation in a subset of *BRAF*-mutant cancer cells characterized by primary resistance to vemurafenib. In these cells, autocrine interleukin-6 (IL-6) secretion may contribute to the primary resistance phenotype via induction of JAK/STAT3 and MAPK signaling. In a subset of cell lines, combined IL-6/MAPK inhibition is able to overcome primary resistance to BRAF-targeted therapy. Overall, we show that the signaling plasticity exerted by primary resistant *BRAF*-mutant cells is achieved by their ability to mimic signaling features of oncogenic RAS, a strategy that we term "oncogene mimicry." This model may guide future strategies for overcoming primary resistance observed in these tumors.

INTRODUCTION

Activating mutations in the serine/threonine kinase BRAF are among the most common genetic lesions across all cancers and leads to RAS-independent induction of mitogen-activated protein kinase (MAPK) signaling in these tumors (Bamford et al., 2004; Davies et al., 2002; Seger and Krebs, 1995). Given the central role of MAPK signaling for tumor growth of *BRAF*-mutant cancers, a multitude of targeted drugs have been developed. In contrast to *KRAS*-mutant tumors, in subgroups of *BRAF*-mutant patients, MAPK pathway inhibitors such as vemurafenib or trametinib have been shown to be clinically active (Chapman et al., 2011; Falchook et al., 2012; Jänne et al., 2013).

The central paradigm in the development of inhibitors of oncogenically driven cancers is that patients harboring kinase mutations are highly likely to benefit from inhibition of the pathway engaged by these kinases. The efficacy of such a targeted approach is commonly limited through selection of cells that are insensitive to the drug (acquired resistance), as observed for BCR-ABL-positive chronic myeloid leukemia tumors treated with imatinib (Shah et al., 2004). Despite dramatic responses in subgroups of melanoma patients, in the case of MAPK pathway inhibitors, the major clinical challenge is the high rate of *BRAF*-mutant tumors that never respond to treatment (primary resistance) (Chapman et al., 2011; Kudchadkar et al., 2012). The finding that $BRAF^{V600E}$ present in different tissues exhibits drastically different sensitivity to vemurafenib suggests drastically different wiring diagrams and adds to the complexity of primary resistance to MAPK pathway inhibition in *BRAF*-mutant tumors (Prahallad et al., 2012).

A great deal of recent effort has been expended to understand the different intrinsic signaling behavior of $BRAF^{V600E}$ cells of different tissues of origin in response to BRAF inhibitors. Rosen and colleagues have uncovered a profound relief of upstream negative feedback upon BRAF inhibition, which explains resistance in melanoma cells (Lito et al., 2012). Other studies identified the EGFR/HER3 pathway as a source of primary resistance signaling that may overcome MAPK pathway inhibition in *BRAF*-mutant cells (Corcoran et al., 2012; Montero-Conde et al., 2013; Prahallad et al., 2012). Intrigued by these observations, we initiated an effort to systematically map the signaling differences between primary resistant and sensitive $BRAF^{V600E}$-mutant cells originating from different tissues.

Our approach relied on two complementary mass spectrometry platforms: (1) a kinase inhibitor bead-based affinity purification to profile active kinases within the MAPK pathway and parallel pathways, and (2) a stable *i*sotope *l*abeling with *a*mino acids in *c*ell culture (SILAC)-based phosphoproteomic analysis to capture the output of a wide variety of signaling outputs. To our knowledge, this is the most comprehensive kinase and phosphoprotein analysis of the primary resistant state of $BRAF^{V600E}$-mutant tumor cells. Our analyses uncover several mechanisms that buffer the drug-induced blockade of MAPK signaling. Furthermore, we show that primary resistant cells, in contrast to the sensitive cells, secrete the cytokine interleukin-6 (IL-6) in

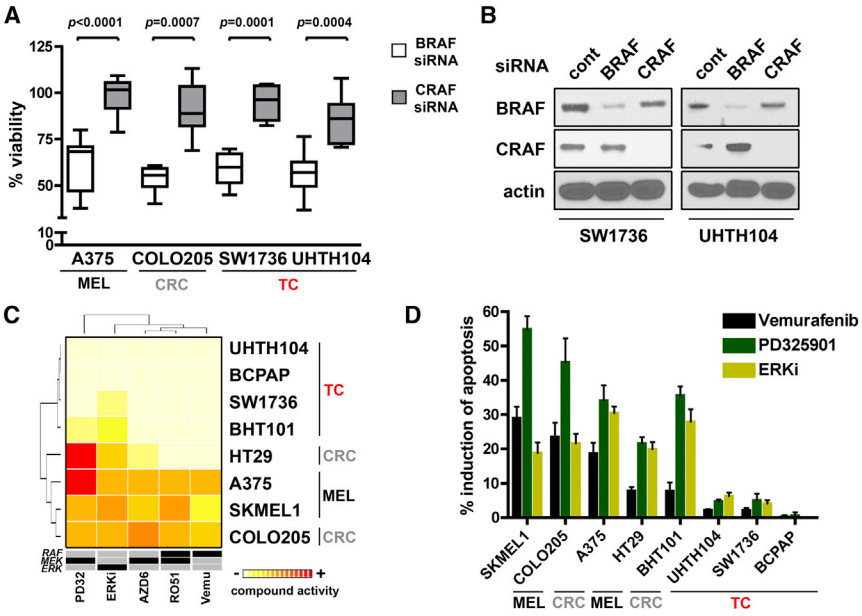

Figure 1. Primary Resistance to MAPK Inhibition in BRAF-Mutant Cancer

(A) Viability of cell lines transfected with either BRAF- (white) or CRAF-siRNA (gray) as compared to control siRNA is displayed. p values (t test) represent statistical significance, and whiskers of boxplots represent SD.

(B) Cells transfected with control-, BRAF-, or CRAF-siRNA were analyzed for BRAF, CRAF, and actin protein expression.

(C) Hierarchical clustering of compound (PD325901, ERKi, AZD6244, RO5126766, and vemurafenib; x axis) activity profiles across *BRAF*^{V600E}-mutant cell lines (CRC, colorectal; MEL, melanoma; TC, thyroid; y axis). Color-coded bars represent compound activity (red, active; white, inactive) bars.

(D) Induction of apoptosis (y axis) after 72 hr treatment with vemurafenib (1 μM), PD325901 (0.1 μM), or ERKi (0.3 μM) is displayed across *BRAF*^{V600E}-mutant cells (CRC, colorectal; MEL, melanoma; TC, thyroid; x axis).

Error bars represent SEM.

an autocrine fashion, which may endow cells with the ability to bypass MAPK pathway inhibition. These findings provide several mechanisms that contribute to the distinction between sensitive and primary resistant *BRAF*^{V600E}-mutant cancer types and their ability to mimic molecular features of *KRAS*-mutant cells to promote resistance signaling. Finally, our results may provide several rational therapies to combine with MAPK pathway inhibitors in order to circumvent primary resistance in subgroups of *BRAF*^{V600E}-mutant tumors.

RESULTS

Primary Resistance to MAPK Inhibition Is Uncoupled from BRAF Dependency

Since sensitivity to MAPK pathway inhibition in *BRAF*-mutant cells has been linked to the individual lineage of the tumor, we first set out to test if BRAF dependency would differ between *BRAF*-mutant cells derived from different tissues (Corcoran et al., 2012; Prahallad et al., 2012). To this end, we depleted BRAF in A375 (melanoma), COLO-205 (colorectal carcinoma), and SW1736 and UHTH104 (thyroid carcinoma) *BRAF*^{V600E}-mutant cells (Figures 1A and 1B). Knockdown of BRAF, but not of its close homolog CRAF, led to a significant ($p < 0.0001$) reduction of cellular viability in all cells (Figures 1A and 1B). Next, we assessed the activity of a series of RAF (vemurafenib, RO5126766), MEK (PD325901, selumetinib), and ERK (A0048-48) inhibitors in a collection of *BRAF*^{V600E}-mutant cell lines. When performing hierarchical clustering of the individual half-maximal inhibitory concentration values, we identified a striking difference in the sensitivity of subgroups of *BRAF*-mutant cells (Figure 1C) with primarily thyroid cancer cells enriched in the group of resistant cells (Figure S1A). This differential vulnerability pattern was also reflected in apoptosis assays performed in cells treated with vemurafenib, PD325901, or A0048-58 (ERKi) (Figure 1D). However, short-term pathway inhibition (1 hr) with the individual compounds resulted in a similar deactivation of MAPK signaling effectors (Figure S1B) and a similar perturbation of the transcriptional output of the pathway (Figure S1C) in sensitive (A375) and resistant (BCPAP and SW1736) cell lines (Pratilas et al., 2009). Overall, these data suggest that BRAF dependency, as determined by small interfering RNA (siRNA) against BRAF, is conserved in *BRAF*-mutant cells. However, the dependency does not correlate with pharmacologic perturbation of the pathway, as a subset of the BRAF-mutant cells (enriched for thyroid carcinoma) displays primary resistance to MAPK pathway inhibition.

MAPK Inhibition Promotes RAS-RAF-MEK Complex Formation and MAPK Hyperactivation in Primary Resistant Cells

Previous studies in *BRAF*-mutant cancers identified loss of feedback inhibition of RAS as a potential source for resistance to RAF-MAPK inhibition and reactivation of the MAPK pathway (Corcoran et al., 2012; Montero-Conde et al., 2013). In line with these studies, we observed induction of RAS activity and subsequent restoration of MAPK pathway signaling as measured by phosphorylation of CRAF and ERK only in MAPK inhibitor-resistant, but not sensitive, cancer cells (Figures 2A and S2A). To test if activated RAS may be causally linked with MAPK pathway reactivation, we overexpressed a wild-type *KRAS* and a mutant *KRAS*^{G12C} allele in *BRAF*-mutant sensitive cells and treated these cells with either PD325901 (Figure 2B) or vemurafenib (Figure S2B). In all scenarios, short-term treatment (1–3 hr) with both drugs led to a robust deactivation of MAPK signaling as measured by phospho-ERK. However, within 24 hr, only cells expressing *KRAS*^{G12C}, but not *KRAS*^{WT}, were able to restore phospho-ERK levels (Figures 2B and S2B). These data suggest that oncogenically activated KRAS can mimic the effects of feedback-activated RAS in its ability to override the MAPK inhibitor-mediated deactivation of ERK. Knockdown of BRAF or KRAS in

two resistant cells validated the importance of RAS/RAF effector activation for the induction of primary resistance to MAPK inhibition (Figures S2C and S2D).

Complex formation of RAF dimers is known to activate MAPK signaling, and thus we hypothesized that drug-induced RAS activation might induce formation of RAS-RAF dimers to promote MAPK pathway reactivation (Rushworth et al., 2006). Indeed, we found that expression of *KRAS*^{G12C} promotes RAS-RAF dimer formation without influencing BRAF-CRAF and BRAF-MEK binding, suggesting that RAS is joining a multimeric complex (Figure 2C). Since drug-induced RAS-RAF complex formation might play a role in MAPK pathway reactivation, we assessed whether drug treatment induces the formation of these complexes in MAPK inhibitor primary resistant *BRAF*-mutant cells in immunoprecipitation assays. These analyses revealed that induction of BRAF-CRAF dimerization correlates with MAPK pathway reactivation in primary resistant, but not in sensitive, cells (Figure S2E). The formation of CRAF-BRAF heterodimers is paralleled by their recruitment to RAS and binding to MEK, resulting in the formation of RAS-RAF-MEK multimers (Figure S2F). This is in contrast to *BRAF*^{V600E}-mutant MAPK inhibitor-sensitive cells, where MEK inhibition does not promote formation of RAS-RAF complexes and does not induce binding of RAF to MEK (Figure 2D). We observed a similar induction of RAS-RAF-MEK complex formation in primary resistant cells treated with either a RAF or an ERK inhibitor (Figure 2E). These data suggest that in primary resistant cells, drug treatment induces a time-dependent formation of RAS-RAF-MEK multimers that ultimately reactivate downstream ERK signaling.

Recent data suggest that the formation of higher-order multimers of RAF kinases might be an important step toward the activation of MAPK signaling (Nan et al., 2013). To identify these higher-order multimers and to further substantiate our observations in immunoprecipitation assays, we developed a small-molecule affinity probe capable of selectively purifying active RAF kinase by coupling sorafenib to Sepharose beads (Figure 2F) (Duncan et al., 2012). Of note, we decided to use sorafenib based on its chemical properties as a tool compound that can be coupled to Sepharose beads. First, we validated the capability of sorafenib beads (SFB-B) to capture activation-induced (via EGF or expression of *BRAF*^{V600E}-mutant allele) accumulation of RAF kinases (SFB-B binding) in human embryonic kidney 293T cells (Figure S3A). Using this method, we identified an MEK inhibitor-induced increase in inhibitor-bead binding affinity for BRAF, CRAF, and also KSR1 in MAPK inhibitor-resistant (SW1736), but not in sensitive (SKMEL1), cells (Figure 2G). Since KSR has been previously described as an essential component of physiological BRAF signaling transduction (Brennan et al., 2011), we hypothesized that the drug-induced KSR1-BRAF binding might play a role in the induction of primary resistance to MAPK inhibition. Indeed, siRNA-mediated silencing of KSR1 expression significantly reduced MAPK pathway reactivation (Figure S3B) and cellular viability of MEK inhibitor-treated cells (SW1736 and UHTH104) (Figures 2H and S3C). Thus, feedback-induced formation of RAS-RAF-MEK multimers may also involve KSR1/RAF complexes that add to the overall phenotype of primary resistance to MAPK inhibition in *BRAF*-mutant cells.

Overriding MAPK Hyperactivation in BRAF-Mutant Primary Resistant Cells

Encouraged by the utility of a single-inhibitor bead to reveal differential kinase activation mechanisms, we next developed a custom-designed *m*ultiplexed kinase *i*nhibitor *b*eads (MIB) library (Duncan et al., 2012; Graves et al., 2013) to systematically detect drug-induced perturbation of kinase signaling in MAPK inhibitor primary resistant SW1736 cells at early (1 hr) and late (24 hr) time points after drug treatment. (Figures S4A and S4B). Using this enrichment method coupled to mass spectrometry-based protein analysis (Figure S4C), we were able to detect 128 unique kinases (Figure 3A; Table S1). In the group of preferentially enriched kinases after PD325901 treatment at both time points, we detected canonical MAPK pathway members (MEK2 and ERK1) and five non-canonical MAPK pathway effectors (MP2K2, M3K2, TAOK2, M4K5, and TAOK3) (Figures 3A and 3B; Table S1). These results suggest the formation of activating complexes between MAPK family members extends beyond those initially identified using our single-inhibitor bead pull-downs and are part of a more global signaling adaptation to overcome the initial inhibitory effect of the drug.

We speculated that the adaptive range of the increased MAPK pathway flux is finite and that high-dose MAPK inhibition may be able to override this primary resistance mechanism. To test this hypothesis, we steadily increased the concentration of PD325901 and measured the ability of the cells to reactivate MAPK signaling (Figure 3C). As expected, in both sensitive cells (A375 and SKMEL1), short-term and long-term MEK inhibition eliminates phospho-ERK, but in primary resistant (SW1736 and UHTH104) cells, phosphorylation of ERK recovers when cells are treated with low-dose (0.1 μM) PD325901 (Figure 3C). In contrast, high-dose (1–10 μM) MEK inhibition prevents recovery of phospho-ERK levels in these cells (Figure 3C). Interestingly, high-dose treatment with vemurafenib does not disrupt reactivation of ERK in these cells, suggesting that the increased pathway flux is only partially dependent on RAF kinase activity (Figure S4D). We observed the same pattern of ERK reactivation following treatment of A375 cells expressing a constitutively active *KRAS*^{G12C} allele (Figure 3D) that mimics the feedback-induced effects of primary resistant cells (Figure 2B). The disruption of MAPK reactivation translates into a dramatic increase in apoptosis, as observed in primary resistant SW1736 and UHTH104 cells treated with PD325901, but not with vemurafenib (Figure 3E).

Consequently, nude mice xenografts generated from primary resistant SW1736 cells remained responsive to PD325901 in a dose-dependent manner, as assessed by tumor volume change over time of treatment (Figure S4E). After 21 days of treatment with either 2 mg/kg (low-dose) or 5 mg/kg (high-dose) PD326901, the high-dose-treated mice showed a higher rate of tumor shrinkage (two out of six) and a significantly ($p = 0.017$) decreased tumor volume when compared to the low-dose-treated cohort (Figures 3F and S4E). Thus, we conclude that in a subset of *BRAF*-mutant tumors, primary resistance to MAPK inhibition is primarily driven by an increased flux of the MAPK signaling that can be overcome by high-dose MEK inhibition.

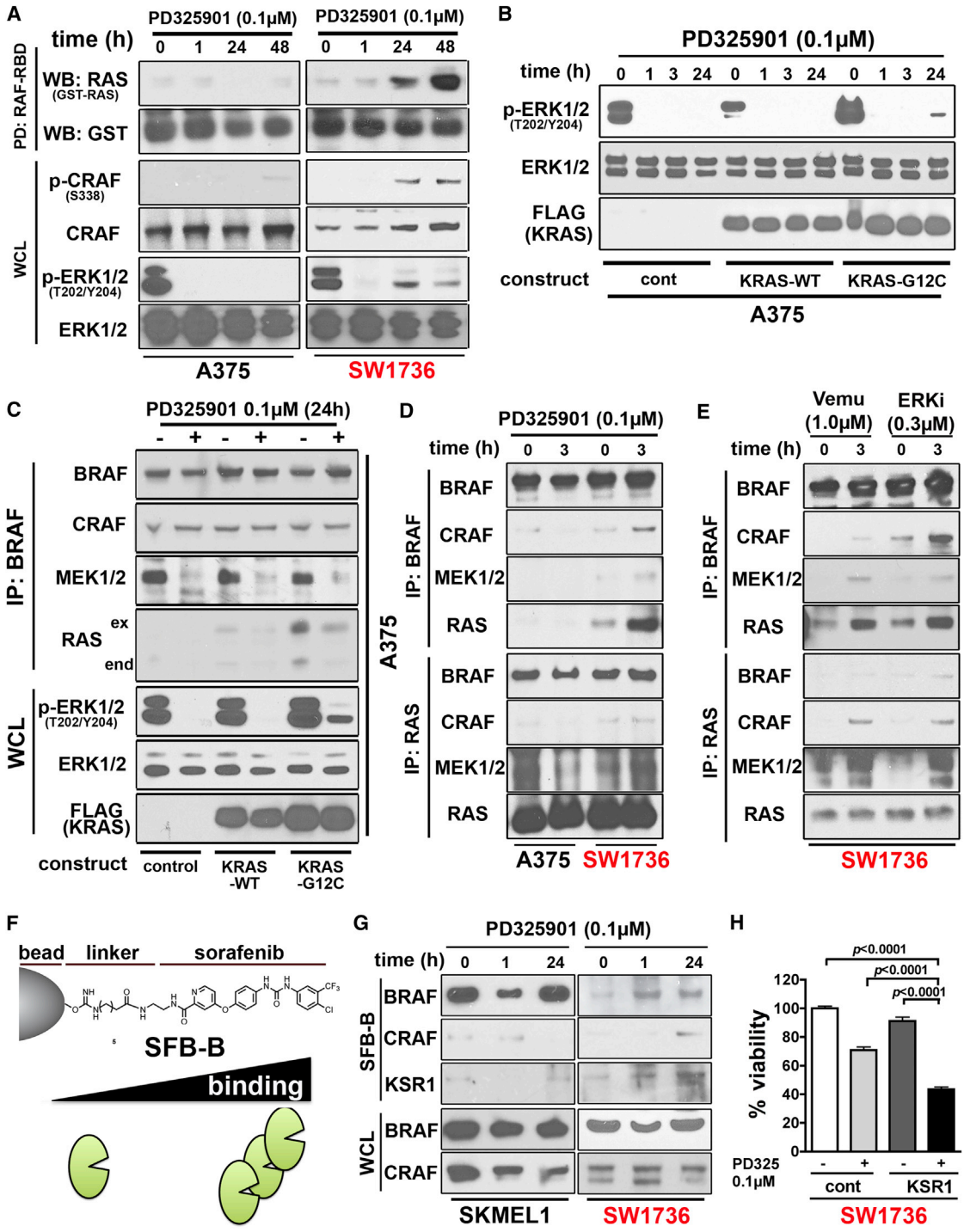

Figure 2. Feedback-Activated RAS Allows Downstream MAPK Pathway Reactivation

(A) Protein levels of cells (sensitive, black; resistant, red) treated with PD325901 (0, 1, 24, and 48 hr) as detected by immunoblotting. RAS-GTP levels were detected by pull-downs of cellular RAS with glutathione S-transferase-tagged RAF1-RBD.

(B) PD325901-treated sensitive A375 cells transfected with control, FLAG-KRAS^{WT}, or FLAG-KRAS^{G12C} were assessed for ERK, phospho-ERK, and FLAG expression. Due to overlapping protein sizes, bands were not detected at the same membrane.

(C) PD325901-treated A375 cells transfected with control, FLAG-KRAS^{WT}, or FLAG-KRAS^{G12C} were assessed for multimers binding to BRAF in immunoprecipitation assays and for ERK, phospho-ERK, and FLAG expression by immunoblotting. Due to overlapping protein sizes, bands were not detected at the same membrane.

(D and E) Sensitive A375 (black) and resistant SW1736 (red) cells treated with (D) PD325901 and (E) vemurafenib or the ERK inhibitor ERKi were assessed for multimers binding to BRAF (upper panel) or RAS (lower panel) in immunoprecipitation assays.

(legend continued on next page)

Systematic Mapping of Adaptation Signaling Reveals Mediators of Primary Resistance

The MIB analysis revealed the set of kinases activated in inhibitor resistant cells. To capture the downstream consequences of kinase reactivation occurring in primary resistant MAPK pathway-reactivated cells, we conducted a SILAC-based mapping of cellular phosphopeptides in SW1736 cells treated with the MEK inhibitor PD325901 over time (0, 1, and 24 hr) (Figure 4A). We identified 3,481 unique phosphopeptides from 1,396 unique proteins (Table S2). Not surprisingly, the abundance of many phosphopeptides decreased after kinase inhibition (Figure 4B). Gene Ontology (GO)-term analysis showed that proteins phosphorylated within 24 hr are significantly enriched in the category of "negative regulation of gene expression" (SG1, immediate increase) and "negative regulation of macromolecule biosynthetic process" (SG2, delayed increase) (Figure 4B; Table S3). Phosphoproteins decreasing in abundance within 24 hr of MEK inhibitor treatment were primarily involved in regulation of the cell cycle (SG3, delayed decrease) and DNA replication (SG4, immediate decrease) (Figure 4B; Table S3). In line with previous reports, we found increased phosphorylation of two receptor tyrosine kinases, ERBB3 and MET (SG1), in the MEK inhibitor-treated SW1736 cells (Figure 4B) (Montero-Conde et al., 2013; Prahallad et al., 2012). Receptor tyrosine kinase (RTK) arrays confirmed MEK inhibitor-induced phosphorylation of not only ERBB3 and MET but also additional RTKs such as EGFR or AXL in resistant (SW1736 and BCPAP), but not in sensitive (A375), cells (Figure 4C). However, we did not observe an increased expression of ERBB3 and EGFR or their respective ligands EGF and NRG1 upon MAPK inhibition (Figure S5A). Interestingly, the treatment with the MET inhibitor crizotinib or the HER2 inhibitor lapatinib (SW1736 and BCPAP) failed to prevent MEK inhibitor-induced reactivation of ERK phosphorylation (Figure S5B). Furthermore, the combination of lapatinib and PD325901 had only a minor effect on the induction of apoptosis in primary resistant cells (Figure S5C). These data suggest that the feedback-induced RTK phosphorylation pattern is not uniform across resistant cells and that inhibition of single nodes of RTK signaling may not be sufficient to prevent feedback-induced MAPK reactivation in *BRAF*-mutant cancer.

We next focused on the group of proteins found to be phosphorylated upon long-term inhibitor treatment (SG2). One of the top-scoring targets of feedback-induced phosphorylation encodes for the nuclear interacting partner of ALK (NIPA) (Figure 4B; Table S2) (Ouyang et al., 2003). In MEK inhibitor-treated SW1736 cells, we identified robust induction of Ser354 phosphorylation, a site that has been identified to be phosphorylated by ERK2. This protein is known to play a role in the regulation of the cell cycle and antiapoptotic signaling (Bassermann et al., 2005; Illert et al., 2012; Ouyang et al., 2003). As expected, MEK inhibition in sensitive A375 cells led to dephosphorylation of NIPA at Ser354 (Figure 4D). However, in primary resistant SW1736 cells, we observed sustained NIPA activation (Figure 4D). Knockdown of NIPA expression via siRNA in SW1736 cells did not affect feedback-induced phosphorylation of ERK (Figure 4E), but NIPA depletion partially enhanced the effects of PD325901 in primary resistant SW1736 cells (Figure 4F). These data indicate that mapping of global signaling adaptation in *BRAF*-mutant cells that have a primary resistance to MAPK inhibition can provide insights into the spectrum of mechanisms that together may render targeted drugs ineffective in these tumors.

Autocrine IL-6 Secretion Defines a Subgroup of Primary Resistant BRAF-Mutant Cells

To further explore the signaling fingerprint of primary resistant SW1736 cells, we focused on the delayed induction of phosphorylation of signal transducer and activator of transcription 3 (STAT3) at Tyr705 (Table S2). Of note, the activation pattern of STAT3 identified in the SILAC assay (Figure 4B) corresponds to the delayed enrichment of JAK3 binding in the MIB assays (Figure 3A), suggesting that the time-dependent reactivation of JAK/STAT signaling is a conserved response to MEK inhibition in these cells. Consistently, MEK inhibition led to increased phosphorylation of STAT3 in two primary resistant cells (BCPAP and SW1736), but not in sensitive A375 cells (Figure 5A). Interestingly, the induction of phosphorylation of STAT3 was only partially dependent on treatment of cells with PD325901-containing media, as treatment with fresh media containing DMSO also led to increased phosphorylation of STAT3 in the resistant cell lines (Figure 5A). Because cytokines such as IL-6 are known activators of STAT3 signaling, we hypothesized that an autocrine loop might be responsible for the time-dependent activation of JAK/STAT signaling (Heinrich et al., 2003). Indeed, we found that over time, increasing IL-6 levels can be detected in the supernatant of resistant cells (BCPAP and SW1736), but not sensitive (A375) cells (Figure 5B). We next assessed IL-6 secretion in all of the initially screened *BRAF*-mutant cells and found a remarkable positive correlation between IL-6 levels and resistance to MAPK inhibitors (Figure 5C). In cytokine arrays, we were able to confirm that IL-6 and CCL5 are secreted at high levels in primary resistant cells (BCPAP and SW1736) when compared to MAPK inhibitor-sensitive A375 cells (Figure 5D). Interestingly, all cells displayed high levels of the IL-6 receptor as measured in fluorescence-activated cell sorting (FACS)-based assays (Figure 5E).

We next asked whether IL-6 might induce resistance in MAPK inhibitor-sensitive A375 cells. The addition of IL-6 into media of A375 cells significantly ($p < 0.0001$ 5 ng/ml; $p < 0.0001$ 25 ng/ml) reduced the induction of apoptosis mediated by PD325901 in a dose-dependent manner as measured in FACS assays (Figure 6A) and induced STAT3 and partial ERK phosphorylation (Figure 6B). These data suggest that autocrine

(F) Schematic presentation of a sorafenib-based (SFB-B) inhibitor beads.
(G) Accumulation of BRAF, CRAF, and KSR1 was assessed in SKMEL1 (sensitive, black; left panel) and SW1736 (sensitive, red; right panel) cells using SFB-B beads in pull-down assays. BRAF, CRAF, and KSR1 were assessed in whole-cell lysates of the given cells.
(H) SW1736 (red, resistant; left panel) cells transfected with control- or KSR1-targeted siRNA treated with either control or PD325901 (48 hr) were assessed for viability. Error bars represent SEM.

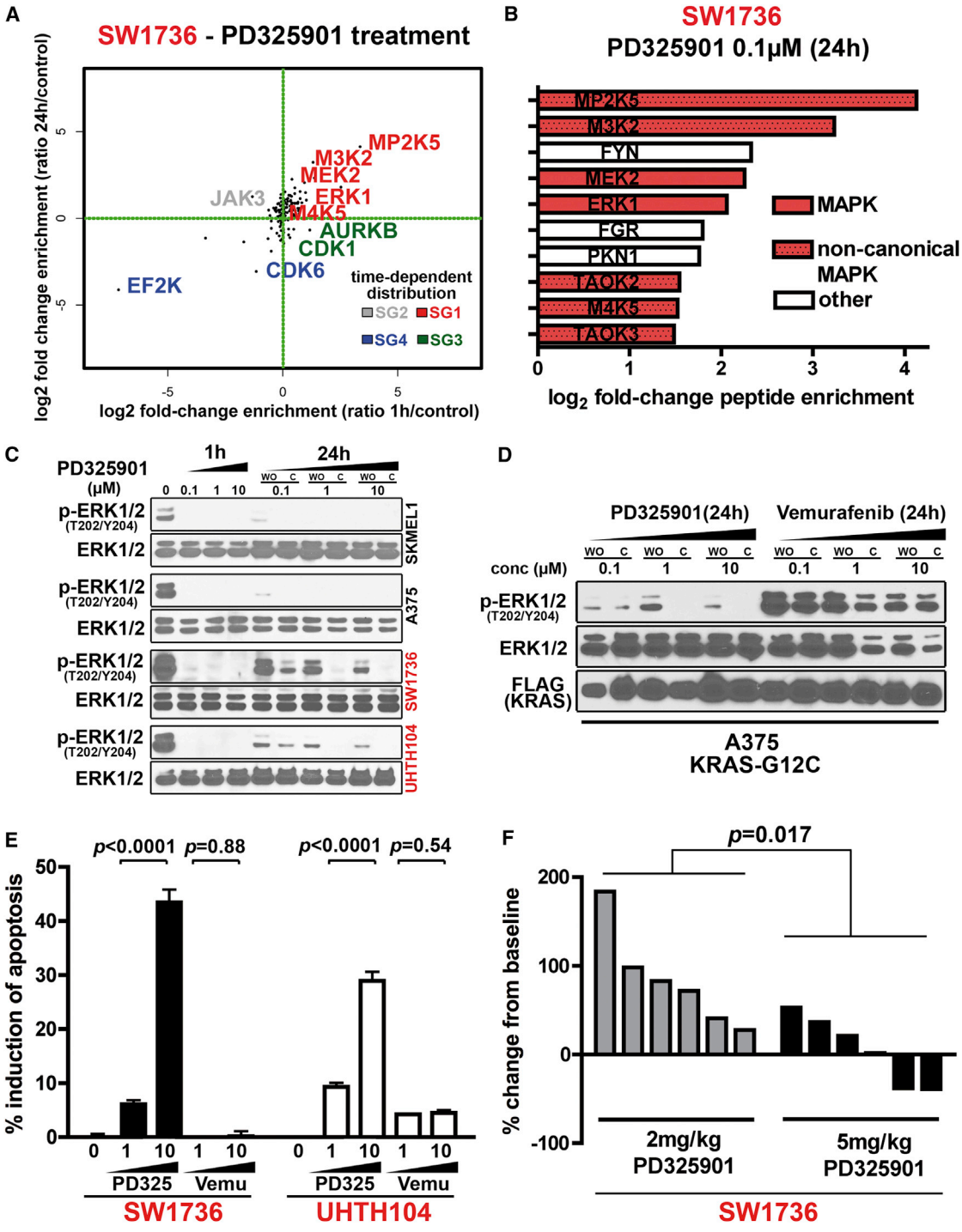

Figure 3. High-Dose MEK Inhibition Prevents Reactivation of MAPK in Primary Resistant Cells

(A) Mapping of all identified kinases (n = 128) according to the log2-change of enrichment as compared to control for cells treated either for 1 hr (x axis) or 24 hr (y axis) with PD325901. Selected proteins in the individual groups (red: SG1, immediate enrichment; gray: SG2, delayed enrichment; blue: SG3, immediate decrease; green: SG4, delayed decrease) are highlighted.

(B) Fold-change enrichment of selected kinases binding to MIBs (log_2-scale) as detected by mass spectrometry in resistant SW1736 cells treated with PD325901 (24 hr). MAPK components are marked in red.

(C) Cells (sensitive, black; resistant, red) were treated with increasing concentrations of PD325901 (1 hr and 24 hr). Cells were either treated for 24 hr ("C") or compound was washed out ("WO") with fresh media after 1 hr treatment. ERK and phospho-ERK levels were assessed in immunoblotting assays.

(legend continued on next page)

IL-6 signaling might play role in the setting of primary resistance to MAPK inhibition in *BRAF*-mutant cells. To validate the importance of IL-6 signaling in primary resistance, we depleted IL-6 in SW1736 and BCPAP cells using siRNA (Figure S6A). Cells transfected with IL-6-targeted siRNA showed significantly increased induction of apoptosis ($p = 0.007$ BCPAP; $p = 0.02$ SW1736) only in combination with MEK inhibitor treatment (Figure 6C), and we found reduced reactivation of STAT3 and partial ERK reactivation in both cell lines when compared to control cells (Figure 6D).

Since clinical JAK inhibitors are available, we tested the efficacy of JAK inhibition in combination with MAPK inhibition in primary resistant cells. Indeed, the combined inhibition of JAK signaling with the pan-JAK inhibitor tofacitinib and MEK signaling with PD325901 resulted in suppression of STAT3 reactivation (Figure 6E) and significantly increased the effect of single-agent MAPK inhibition in two out of three resistant cell lines (Figures 6F and S6B). Overall, our data demonstrate that a subset of primary resistant *BRAF*-mutant cells is defined by autocrine cytokine signaling that may guide the choice of combinatorial strategies for the effective treatment of these tumors.

DISCUSSION

Our chemical proteomics approach to dissect global signaling networks in *BRAF*-mutant cells revealed two major mechanisms that contribute to primary resistance: (1) in primary resistant cells, MAPK pathway inhibition can induce RAS-RAF-MEK complex formation that buffers inhibition of the pathway and shifts cellular sensitivity to high-dose MEK inhibition; and (2) autocrine IL-6 secretion and subsequent activation of JAK/STAT signaling represent an unexpected route to overcome targeted inhibition of the MAPK pathway. Both strategies resemble the adaptation mechanisms by which *KRAS*-mutant cells escape targeted inhibition of MAPK signaling, and thus we propose to name this primary resistance concept "oncogene mimicry."

Previous studies have implicated paradoxical RAF dimerization as a source for primary resistance to RAF inhibitors in *BRAF* wild-type cells (Heidorn et al., 2010; Poulikakos et al., 2010). This model elegantly predicted activated RAS as a potential source for RAF inhibitor resistance in *BRAF*-mutant cells (Poulikakos et al., 2010). Our analyses expand this mechanistic model by revealing that activated RAS facilitates formation of RAS-RAF-MEK complexes that allow hyperactivation of the upstream pathway and reactivation of ERK signaling independently of direct RAF kinase inhibition. Using kinase inhibitor beads, we were able to show that in *BRAF*-mutant cells, MAPK inhibition can release negative feedback loops to activate BRAF, CRAF, KSR, and potentially noncanonical members of the MAPK pathway. Overall, the resulting perturbation of RAS/RAF signaling in response to MAPK pathway inhibition in primary resistant $BRAF^{V600E}$-mutant cells largely resembles the paradoxical activation of RAF signaling found in *KRAS*-mutant cells (Heidorn et al., 2010; Poulikakos et al., 2010). In line with previous reports, we identify RTK signaling as a target of negative feedback loop release (Corcoran et al., 2012; Montero-Conde et al., 2013). However, our data suggest that the inhibition of single RTK nodes may not be sufficient to override primary resistance to MAPK pathway inhibition in *BRAF*-mutant tumors.

Furthermore, our results demonstrate that a drug-induced increase in pathway flux can shift the therapeutic window for effective tumor shrinkage of *BRAF*-mutant cancers to high-dose MEK inhibitor treatment regimens. The feasibility of high-dose MEK treatment of *BRAF*-mutant patients is limited by potential toxicities at doses higher than the given maximum tolerated dose; however, strategies like intermittent high-dose scheduling of targeted drugs have been proven to be effective in other scenarios (Amin et al., 2010) and may be applicable for subgroups of primary resistant cancer patients.

Building on previous studies, our data further highlight the value of chemoproteomic analyses for the dissection of signaling networks perturbed by highly selective kinase inhibitors (Duncan et al., 2012; Graves et al., 2013). In a subset of cell lines, we were able to identify activation of NIPA as well as autocrine IL-6 signaling as potential mediators of primary resistance to RAF inhibition in *BRAF*-mutant cancer. The identification of IL-6 signaling adds to the list of signaling nodes that can mediate primary resistance upon exposure to their receptor ligands (Lito et al., 2012; Wilson et al., 2012). Importantly, IL-6 secretion has been previously reported to play a role in acquired resistance to selumetinib in a $BRAF^{V600E}$-mutant model of childhood astrocytoma (Bid et al., 2013). Future studies may be able to clarify how much the lineage determines the ability of the cell to secrete individual cytokines such as IL-6. Furthermore, autocrine secretion of IL-6 and other cytokines has been reported to play a major role in the activation of oncogenic signaling in RAS-dependent cells (Ancrile et al., 2007; Zhu et al., 2014). Thus, autocrine cytokine secretion may represent a previously underappreciated source of cancer signaling that adds to the ability of primary resistant *BRAF*-mutant cells to phenocopy *KRAS*-mutant cells and to overcome targeted MAPK pathway inhibition. It remains to be determined how IL-6 signaling is connected with the individual components of the RAS-RAF pathway and whether inhibition of its downstream effectors can be effective to resensitize *BRAF*-mutant cells to RAF inhibitors.

(D) A375 cells were transfected with FLAG-$KRAS^{G12C}$ and were treated with either PD325901 or vemurafenib for 24 hr ("C") or compound was washed out ("WO") with fresh media after 1 hr treatment. ERK and phospho-ERK levels were assessed in immunoblotting assays. Due to overlapping protein sizes, bands were not detected at the same membrane.

(E) Induction of apoptosis (y axis) after 72 hr treatment with either PD325901 (0, 1, and 10 μM) or vemurafenib (0, 1, and 10 μM) is displayed for resistant (red) SW1736 and UHTH104 cells.

(F) Change of tumor volume form baseline (y axis) for individual xenograft tumors of SW1736 cells treated with either 2 mg/kg (gray bars) or 5 mg/kg of PD325901 (black bars) were measured at day 21. p values indicate the statistical significance between the mean change in tumor volumes.

Error bars represent SEM.

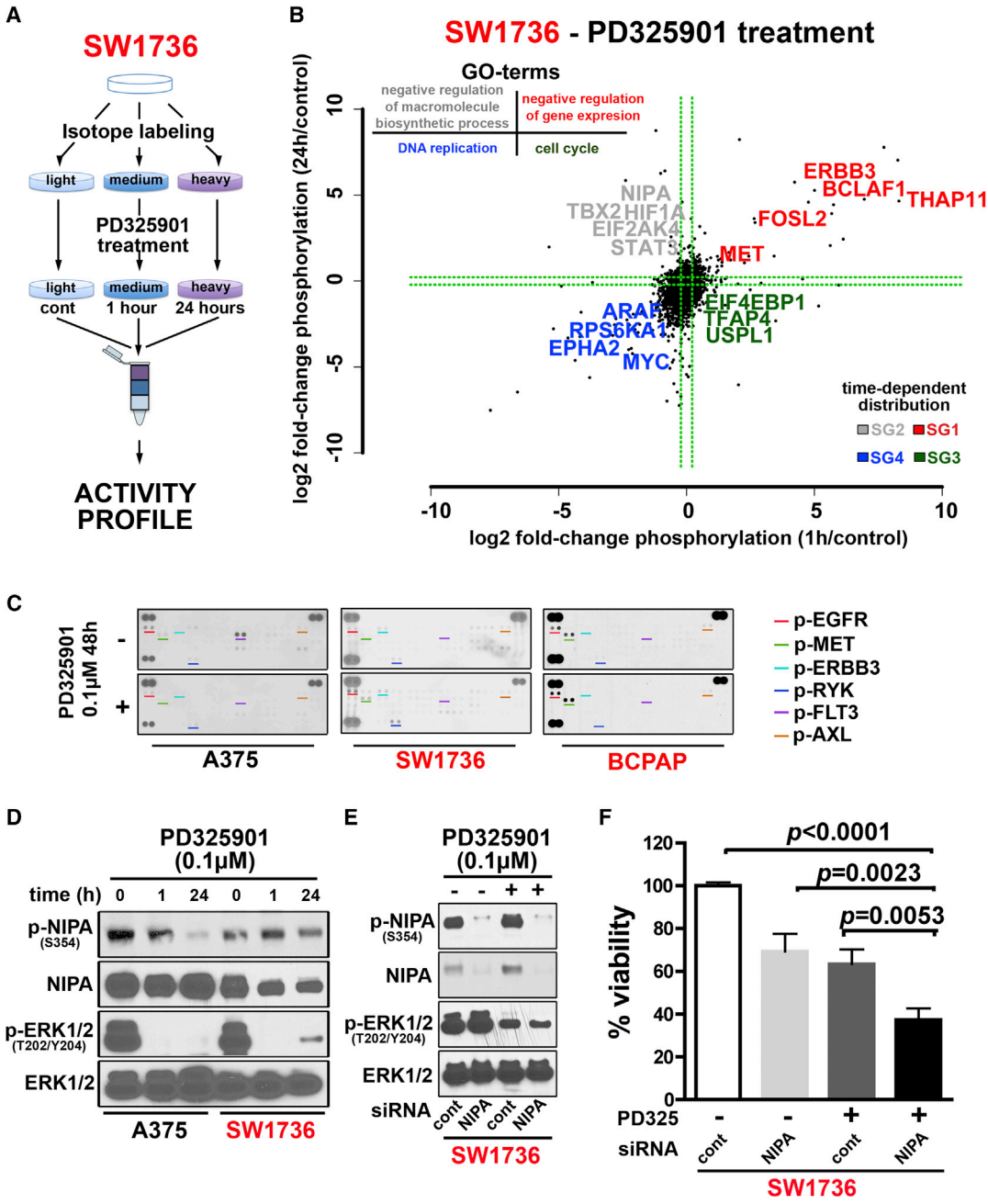

Figure 4. Mapping of Global Phosphoproteome Perturbation Reveals Effectors of Primary Resistance in BRAF-Mutant Cells

(A) Graphic overview of the isotope-labeling strategy for SILAC-based detection of phosphoproteome activity.

(B) Mapping of all identified phosphopeptides according to the log2-change of phosphorylation levels as compared to control for cells treated for either 1 hr (x axis) or 24 hr (y axis) with PD325901. Selected proteins in the individual groups (red, SG1; gray, SG2; blue, SG3; green, SG4) are highlighted. Inlay panel (upper left corner) shows the top-scoring GO-term annotation for the individual groups.

(C) Sensitive (black; A375) and resistant (red; SW1736, BCPAP) cells were treated with PD325901 (0 and 48 hr), and phosphorylation status of 49 RTKs was detected using RTK arrays. Selected RTKs are highlighted.

(D) Sensitive (black, A375) and resistant (red, SW1736) cells treated with PD32590 (0, 1, and 24 hr) were analyzed for protein expression of phospho-NIPA, NIPA, phospho-ERK, and ERK.

(E) SW1736 cells transfected with control- or NIPA-targeted siRNA treated either with control or PD325901 (24 hr) were assessed for expression of phospho-NIPA, NIPA, ERK, and phospho-ERK.

(F) Viability (y axis) of SW1736 cells treated with either control (–) or PD325901 for 48 hr (+) transfected with either control (white, dark gray) or NIPA (light gray, black) is displayed.

Statistical significance (Student's t test) between the average viability of given cells is displayed as p values, and error bars represent SEM.

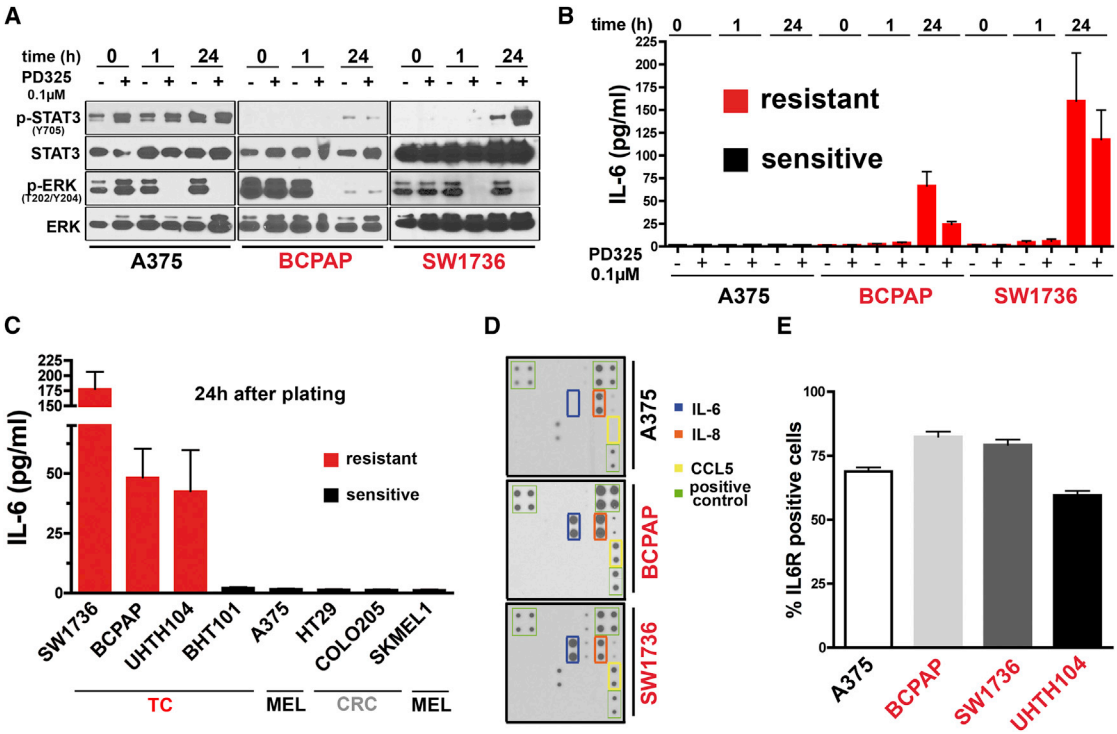

Figure 5. Autocrine IL-6 Signaling Defines a Subset of Primary Resistant *BRAF*-Mutant Cells

(A) Sensitive (black; A375) and resistant (red; SW1736, BCPAP) cells treated with fresh media containing either DMSO (0, 1, and 24 hr) or PD32590 (0, 1, and 24 hr) were analyzed for protein expression of phospho-STAT3, STAT3, phospho-ERK, and ERK.

(B) Supernatants of sensitive (black; A375) and resistant (red; SW1736, BCPAP) cells treated with fresh media containing either DMSO (0, 1, and 24 hr) or PD32590 (0, 1, and 24 hr) were analyzed for IL-6 secretion (y axis) using ELISA assays. Error bars represent SEM.

(C) Analysis of IL-6 secretion (y axis) of $BRAF^{V600E}$-mutant cells (red, resistant; black sensitive) into media 24 hr after plating. Error bars represent SEM.

(D) Supernatants of sensitive (black; A375) and resistant (red; SW1736, BCPAP) cells were analyzed for 23 distinct cytokines using cytokine arrays. Selected cytokines and positive controls are highlighted.

(E) Sensitive (black; A375) and resistant (red; BCPAP, SW1736, UHTH104) cells were assessed for expression of the IL-6 receptor in FACS-based assays. Error bars represent SEM.

Overall, we show that the dissection of drug-induced negative feedback loop networks can provide important insights into the dynamics of primary resistant signaling in *BRAF*-mutant cancer. Future analyses of patient samples may potentially allow translating these findings into the development of novel therapeutic strategies to further increase the response rates to RAF inhibitors in *BRAF*-mutant patients.

EXPERIMENTAL PROCEDURES

Cell Lines and Reagents

Cell lines were obtained from the ATCC (http://www.atcc.org) or received as a kind gift from Dr. Fagin (SW1736) or Dr. Nils-Erik Heldin (UHTH104) and were cultured using either RPMI or Dulbecco's modified Eagle's medium cell culture media, supplemented with 10% fetal bovine serum (FBS). All compounds were purchased from commercial suppliers or kindly provided by Dr. Pingda Ren (A0048-58, ERKi). Recombinant IL-6 (Peprotech) was diluted in water and stored at −80°C.

Viability Assays

Cell lines were plated in triplicates into 96-well plates (1,000–2,000 cells/well) and treated with the given compounds. Viability was determined after 48–72 hr by measuring the ATP-content (CellTiter-Glo, Promega), and the percentage of viable cells as compared to DMSO controls was calculated as described previously (Sos et al., 2009). Half-maximal inhibitory concentration (EC_{50}) was assessed using nonlinear curve-fitting algorithms (Prism).

Apoptosis Assays

For detection of apoptosis, the Annexin V-FITC Apoptosis Detection Kit I (BD Biosciences) was used and analysis was performed as described previously (Sos et al., 2009). Briefly, cells were treated with the given compound (72 hr) and stained with Annexin V-FITC and propidium iodide before analysis on a FACS LSRII (Beckman Coulter). Apoptosis was calculated as the difference between treated sample and DMSO control. At least 10,000 cells were measured per sample.

Immunoblotting, Immunoprecipitation, and RTK Arrays

Cells were treated at given conditions and lysed in phosphatase and protease inhibitor containing lysis buffer (Cell Signaling). Samples were run on SDS-PAGE gels (Life Sciences). All antibodies are listed in Supplemental Experimental Procedures. For immunoblotting, lysates were mixed with BRAF (Santa Cruz, B-7) or Ras antibody (Abcam, EPR3255) and incubated overnight (4°C). Protein G agarose beads were used to capture complex formation, and samples were subjected to SDS-PAGE. For RTK-array experiments, prewashed RTK membranes (R&D Systems) were incubated with cell lysates (150–200 μg protein) and chemiluminescent signals were detected on X-ray films according to the manufacturer's instructions.

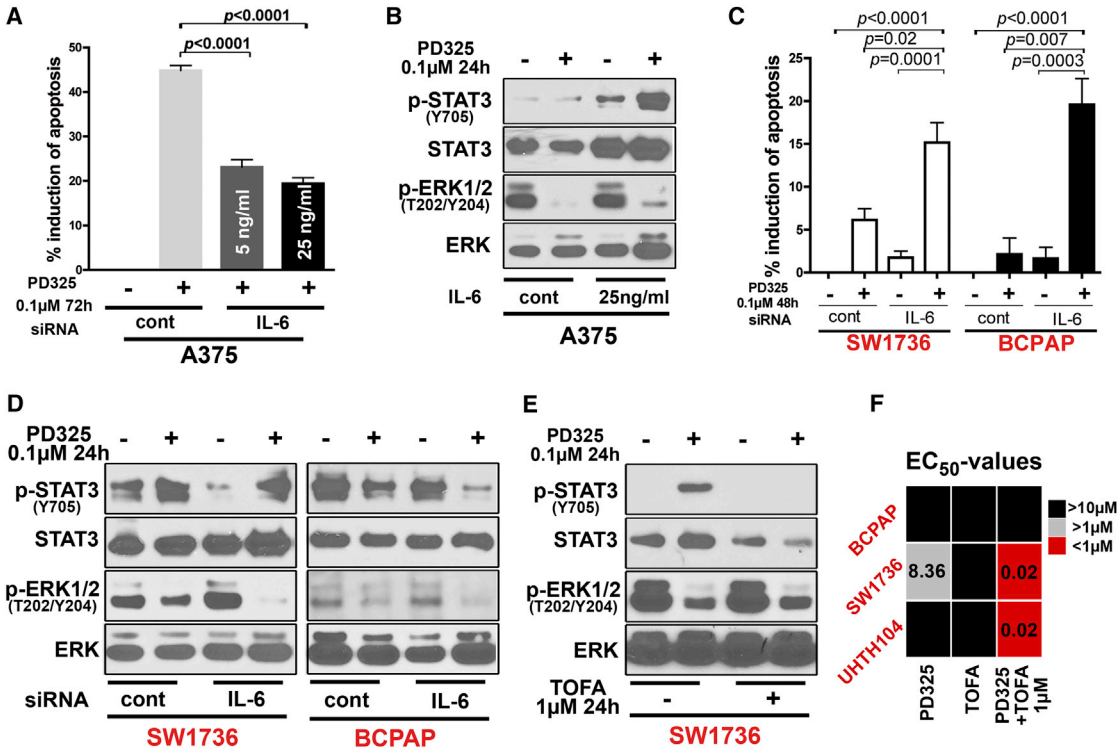

Figure 6. IL-6 Secretion Sensitizes Primary Resistant Cells to Combined IL-6/MAPK Pathway Inhibition

(A) Induction of apoptosis after 72 hr treatment with either PD325901 (0.1 μM) alone or PD325901 (0.1μM) in combination with IL-6 (5 ng/ml, 25 ng/ml) is displayed for A375 cells. Error bars represent SEM.

(B) A375 cells treated (24 hr) either with control (±IL-6, 25 ng/ml) or PD325901 (±IL-6, 25 ng/ml) were assessed for expression of phospho-STAT3, STAT3, ERK, and phospho-ERK. Due to overlapping protein sizes, bands were not detected at the same membrane.

(C) Induction of apoptosis after 48 hr treatment with either PD325901 (0.1 μM) alone or PD325901 (0.1 μM) ±IL-6 depletion (siRNA; 72 hr) is displayed for SW1736 and BCPAP cells. Error bars represent SEM.

(D) SW1736 and BCPAP cells treated (24 hr) either with control (±IL-6 siRNA) or PD325901 (±IL-6 siRNA) were assessed for expression of phospho-STAT3, STAT3, ERK, and phospho-ERK. Due to overlapping protein sizes, bands were not detected at the same membrane.

(E) SW1736 cells treated (24 hr) with either control (±1 μM tofacitinib) or PD325901 (±1 μM tofacitinib) were assessed for expression of phospho-STAT3, STAT3, ERK, and phospho-ERK. Due to overlapping protein sizes, bands were not detected at the same membrane.

(F) EC_{50} values (EC_{50} > 10 μM, black; EC_{50} > 1 μM, gray; EC_{50} < 1 μM, red) as assessed by viability assays are displayed for the given cell lines treated with PD325901, tofacitinib, or a combination of both inhibitors (1 μM tofacitinib constant).

RNAi and Transient Overexpression

Cells were plated (50%–80% confluency) 24 hr prior to transfection with either the siRNA construct (Lipofectamine RNAiMAX) or the plasmid (Lipofectamine LTX). All transfection reagents were diluted in serum-free OPTI-MEM media according to the manufacturer's instructions. Codon-optimized pJ603-neo-KRAS (DNA 2.0) and pcDNA3-BRAF constructs were used for transient expression experiments.

SILAC-Based Phosphoproteomics Strategy Overview

SILAC labeling, mass spectrometry (MS), and data processing for a single experiment are described in detail in Supplemental Experimental Procedures. Briefly, cells were metabolically labeled for seven doubling times in RPMI with 10% dialyzed FBS supplemented with heavy (13C6, 15N2-Lys, 13C6, and 15N4-Arg), medium (2H4-Lys and 13C6-Arg), or light (unlabeled Lys and Arg) amino acids (Thermo Scientific). After compound treatment, cells were harvested, washed, and lysed in the presence of phosphatase inhibitors, and equal amounts of protein were combined and digested overnight with sequencing grade modified trypsin (Promega). Phosphopeptides were enriched by titanium oxide chromatography. MS analysis was performed in an Orbitrap Velos as described in the supplemental information. Data were searched against the human subset of the SwissProt database using Protein Prospector (Clauser et al., 1999), as described in Supplemental Experimental Procedures. Ratios of peptide peak areas between conditions were calculated, along with variance for each ratio. Plots of calculated ratios were generated in "R."

MIB-Based Phosphoproteomics Strategy Overview

Compounds were purchased commercially (dasatinib, crizotinib, staurosporine, SB202190, and lapatinib, Selleck Chemicals; purvalanol B, Tocris; bisindolylmaleimide X, Enzo Life Sciences). Linkable versions of previously described compounds were synthesized based on prior methods; VI-16832l (Daub et al., 2008), Akti-46 (Blake et al., 2010), PP-hydroxyl (Tanaka et al., 2005), sorafenib (Bankston et al., 2001), and JG-4 (Statsuk et al., 2008); purvalanol B was coupled to ether-linked 1,6-diaminohexane Sepharose and all others to ECH following prior methods, with quenching with acetic acid or ethanolamine, respectively (Duncan et al., 2012). Kinase enrichment was performed as described previously (Cooper et al., 2013; Duncan et al., 2012). A detailed description of the phosphoproteomic strategy for MIB data generation for a single experiment is given in Supplemental Experimental Procedures (Schilling et al., 2012). Plots of calculated ratios were generated in "R."

Statistical Analysis

All experiments were repeated at least three times unless specified otherwise. Error bars represent SEM, and p values represent statistical significance

as assessed with a t test implemented in Prism (GraphPad) unless stated otherwise.

IL-6 ELISA Assays and Cytokine Arrays

Supernatants of cells were collected at the indicated time points, and IL-6 was detected in coated 96-well plates using IL-6 ELISA kits (eBioscience) following the manufacturer's instructions. Cytokine arrays (Raybiotech) were incubated with cell-free supernatant overnight, and the signal was detected using chemiluminescent signaling on X-ray film according to the manufacturer's instructions.

Xenograft Mouse Models

Female 7- to 9-week-old Nu/Nu mice (Harlan, FoxN1/nude) were inoculated subcutaneously with 10^7 SW1736 cells. Mice were monitored according to the protocol approved by the UCSF Institutional Animal Care and Use Committee. Each animal received two tumors into the left and right flank. At tumor volumes of 100–200 mm^3, mice orally received PD325901 or vehicle daily. Tumor size was monitored regularly by measurement of perpendicular diameters by an external caliper, and tumor size (mm^3) was calculated as V = 1/2 (length × $width^2$). Animals were monitored for the absence of drug toxicity by measuring the body weight twice weekly and monitoring the overall activity.

ACCESSION NUMBERS

The raw SILAC data can be accessed via http://prospector2.ucsf.edu/prospector/cgi-bin/msform.cgi?form=msviewer using the search key qqj3gxjzkf. The raw MIB data can be accessed via http://prospector2.ucsf.edu/prospector/cgi-bin/msform.cgi?form=msviewer using the search key 4pljxgoury.

SUPPLEMENTAL INFORMATION

Supplemental Information includes Supplemental Experimental Procedures, six figures, and three tables and can be found with this article online at http://dx.doi.org/10.1016/j.celrep.2014.07.010.

ACKNOWLEDGMENTS

We thank Drs. Jesse Lipp, Arvin Dar, and Nicholas Hertz for fruitful discussions. M.L.S. received a Young Investigator Award from the Prostate Cancer Foundation (PCF). This work was supported by the Samuel Waxman Cancer Research Foundation (CA-0052023; K.M.S.), the NIH (CHLA#479/Prime: P01 CA081403, to K.M.S.), and by a Stand Up to Cancer - Prostate Cancer Foundation - Prostate Dream Team Translational Cancer Research Grant. This research grant is made possible by the generous support of the Movember Foundation. Stand Up To Cancer is a program of the Entertainment Industry Foundation administered by the American Association for Cancer Research (K.M.S.). Mass spectrometry was provided by the Bio-Organic Biomedical Mass Spectrometry Resource at UCSF (A.L. Burlingame, director) supported by the Biomedical Technology Research Centers program of the NIH National Institute of General Medical Sciences, NIH NIGMS 8P41GM103481. This publication was made possible with help from the University of California San Francisco-Gladstone Institute of Virology & Immunology Center for AIDS Research (CFAR), an NIH-funded program (P30 AI027763).

Received: March 14, 2014
Revised: May 14, 2014
Accepted: July 10, 2014
Published: August 7, 2014

REFERENCES

Amin, D.N., Sergina, N., Ahuja, D., McMahon, M., Blair, J.A., Wang, D., Hann, B., Koch, K.M., Shokat, K.M., and Moasser, M.M. (2010). Resiliency and vulnerability in the HER2-HER3 tumorigenic driver. Sci. Transl. Med. *2*, ra7.

Ancrile, B., Lim, K.H., and Counter, C.M. (2007). Oncogenic Ras-induced secretion of IL6 is required for tumorigenesis. Genes Dev. *21*, 1714–1719.

Bamford, S., Dawson, E., Forbes, S., Clements, J., Pettett, R., Dogan, A., Flanagan, A., Teague, J., Futreal, P.A., Stratton, M.R., and Wooster, R. (2004). The COSMIC (Catalogue of Somatic Mutations in Cancer) database and website. Br. J. Cancer *91*, 355–358.

Bankston, D., Dumas, J., Natero, R., Riedl, B., Monahan, M.-K., and Sibley, R. (2001). A scaleable synthesis of BAY 43-9006: a potent Raf kinase inhibitor for the treatment of cancer. Org. Process Res. Dev. *6*, 777–781.

Bassermann, F., von Klitzing, C., Münch, S., Bai, R.Y., Kawaguchi, H., Morris, S.W., Peschel, C., and Duyster, J. (2005). NIPA defines an SCF-type mammalian E3 ligase that regulates mitotic entry. Cell *122*, 45–57.

Bid, H.K., Kibler, A., Phelps, D.A., Manap, S., Xiao, L., Lin, J., Capper, D., Oswald, D., Geier, B., DeWire, M., et al. (2013). Development, characterization, and reversal of acquired resistance to the MEK1 inhibitor selumetinib (AZD6244) in an in vivo model of childhood astrocytoma. Clin. Cancer Res. *19*, 6716–6729.

Blake, J.F., Kallan, N.C., Xiao, D., Xu, R., Bencsik, J.R., Skelton, N.J., Spencer, K.L., Mitchell, I.S., Woessner, R.D., Gloor, S.L., et al. (2010). Discovery of pyrrolopyrimidine inhibitors of Akt. Bioorg. Med. Chem. Lett. *20*, 5607–5612.

Brennan, D.F., Dar, A.C., Hertz, N.T., Chao, W.C., Burlingame, A.L., Shokat, K.M., and Barford, D. (2011). A Raf-induced allosteric transition of KSR stimulates phosphorylation of MEK. Nature *472*, 366–369.

Chapman, P.B., Hauschild, A., Robert, C., Haanen, J.B., Ascierto, P., Larkin, J., Dummer, R., Garbe, C., Testori, A., Maio, M., et al.; BRIM-3 Study Group (2011). Improved survival with vemurafenib in melanoma with BRAF V600E mutation. N. Engl. J. Med. *364*, 2507–2516.

Clauser, K.R., Baker, P., and Burlingame, A.L. (1999). Role of accurate mass measurement (+/- 10 ppm) in protein identification strategies employing MS or MS/MS and database searching. Anal. Chem. *71*, 2871–2882.

Corcoran, R.B., Ebi, H., Turke, A.B., Coffee, E.M., Nishino, M., Cogdill, A.P., Brown, R.D., Della Pelle, P., Dias-Santagata, D., Hung, K.E., et al. (2012). EGFR-mediated re-activation of MAPK signaling contributes to insensitivity of BRAF mutant colorectal cancers to RAF inhibition with vemurafenib. Cancer Discov. *2*, 227–235.

Cooper, M.J., Cox, N.J., Zimmerman, E.I., Dewar, B.J., Duncan, J.S., Whittle, M.C., Nguyen, T.A., Jones, L.S., Ghose Roy, S., Smalley, D.M., et al. (2013). Application of multiplexed kinase inhibitor beads to study kinome adaptations in drug-resistant leukemia. PLoS One *8*, e66755.

Daub, H., Olsen, J.V., Bairlein, M., Gnad, F., Oppermann, F.S., Körner, R., Greff, Z., Kéri, G., Stemmann, O., and Mann, M. (2008). Kinase-selective enrichment enables quantitative phosphoproteomics of the kinome across the cell cycle. Mol. Cell *31*, 438–448.

Davies, H., Bignell, G.R., Cox, C., Stephens, P., Edkins, S., Clegg, S., Teague, J., Woffendin, H., Garnett, M.J., Bottomley, W., et al. (2002). Mutations of the BRAF gene in human cancer. Nature *417*, 949–954.

Duncan, J.S., Whittle, M.C., Nakamura, K., Abell, A.N., Midland, A.A., Zawistowski, J.S., Johnson, N.L., Granger, D.A., Jordan, N.V., Darr, D.B., et al. (2012). Dynamic reprogramming of the kinome in response to targeted MEK inhibition in triple-negative breast cancer. Cell *149*, 307–321.

Falchook, G.S., Lewis, K.D., Infante, J.R., Gordon, M.S., Vogelzang, N.J., DeMarini, D.J., Sun, P., Moy, C., Szabo, S.A., Roadcap, L.T., et al. (2012). Activity of the oral MEK inhibitor trametinib in patients with advanced melanoma: a phase 1 dose-escalation trial. Lancet Oncol. *13*, 782–789.

Graves, L.M., Duncan, J.S., Whittle, M.C., and Johnson, G.L. (2013). The dynamic nature of the kinome. Biochem. J. *450*, 1–8.

Heidorn, S.J., Milagre, C., Whittaker, S., Nourry, A., Niculescu-Duvas, I., Dhomen, N., Hussain, J., Reis-Filho, J.S., Springer, C.J., Pritchard, C., and Marais, R. (2010). Kinase-dead BRAF and oncogenic RAS cooperate to drive tumor progression through CRAF. Cell *140*, 209–221.

Heinrich, P.C., Behrmann, I., Haan, S., Hermanns, H.M., Müller-Newen, G., and Schaper, F. (2003). Principles of interleukin (IL)-6-type cytokine signalling and its regulation. Biochem. J. *374*, 1–20.

Illert, A.L., Zech, M., Moll, C., Albers, C., Kreutmair, S., Peschel, C., Bassermann, F., and Duyster, J. (2012). Extracellular signal-regulated kinase 2

(ERK2) mediates phosphorylation and inactivation of nuclear interaction partner of anaplastic lymphoma kinase (NIPA) at G2/M. J. Biol. Chem. *287*, 37997–38005.

Jänne, P.A., Shaw, A.T., Pereira, J.R., Jeannin, G., Vansteenkiste, J., Barrios, C., Franke, F.A., Grinsted, L., Zazulina, V., Smith, P., et al. (2013). Selumetinib plus docetaxel for KRAS-mutant advanced non-small-cell lung cancer: a randomised, multicentre, placebo-controlled, phase 2 study. Lancet Oncol. *14*, 38–47.

Kudchadkar, R., Paraiso, K.H., and Smalley, K.S. (2012). Targeting mutant BRAF in melanoma: current status and future development of combination therapy strategies. Cancer J. *18*, 124–131.

Lito, P., Pratilas, C.A., Joseph, E.W., Tadi, M., Halilovic, E., Zubrowski, M., Huang, A., Wong, W.L., Callahan, M.K., Merghoub, T., et al. (2012). Relief of profound feedback inhibition of mitogenic signaling by RAF inhibitors attenuates their activity in BRAFV600E melanomas. Cancer Cell *22*, 668–682.

Montero-Conde, C., Ruiz-Llorente, S., Dominguez, J.M., Knauf, J.A., Viale, A., Sherman, E.J., Ryder, M., Ghossein, R.A., Rosen, N., and Fagin, J.A. (2013). Relief of feedback inhibition of HER3 transcription by RAF and MEK inhibitors attenuates their antitumor effects in BRAF-mutant thyroid carcinomas. Cancer Discov. *3*, 520–533.

Nan, X., Collisson, E.A., Lewis, S., Huang, J., Tamgüney, T.M., Liphardt, J.T., McCormick, F., Gray, J.W., and Chu, S. (2013). Single-molecule superresolution imaging allows quantitative analysis of RAF multimer formation and signaling. Proc. Natl. Acad. Sci. USA *110*, 18519–18524.

Ouyang, T., Bai, R.Y., Bassermann, F., von Klitzing, C., Klumpen, S., Miething, C., Morris, S.W., Peschel, C., and Duyster, J. (2003). Identification and characterization of a nuclear interacting partner of anaplastic lymphoma kinase (NIPA). J. Biol. Chem. *278*, 30028–30036.

Poulikakos, P.I., Zhang, C., Bollag, G., Shokat, K.M., and Rosen, N. (2010). RAF inhibitors transactivate RAF dimers and ERK signalling in cells with wild-type BRAF. Nature *464*, 427–430.

Prahallad, A., Sun, C., Huang, S., Di Nicolantonio, F., Salazar, R., Zecchin, D., Beijersbergen, R.L., Bardelli, A., and Bernards, R. (2012). Unresponsiveness of colon cancer to BRAF(V600E) inhibition through feedback activation of EGFR. Nature *483*, 100–103.

Pratilas, C.A., Taylor, B.S., Ye, Q., Viale, A., Sander, C., Solit, D.B., and Rosen, N. (2009). (V600E)BRAF is associated with disabled feedback inhibition of RAF-MEK signaling and elevated transcriptional output of the pathway. Proc. Natl. Acad. Sci. USA *106*, 4519–4524.

Rushworth, L.K., Hindley, A.D., O'Neill, E., and Kolch, W. (2006). Regulation and role of Raf-1/B-Raf heterodimerization. Mol. Cell. Biol. *26*, 2262–2272.

Schilling, B., Rardin, M.J., MacLean, B.X., Zawadzka, A.M., Frewen, B.E., Cusack, M.P., Sorensen, D.J., Bereman, M.S., Jing, E., Wu, C.C., et al. (2012). Platform-independent and label-free quantitation of proteomic data using MS1 extracted ion chromatograms in skyline: application to protein acetylation and phosphorylation. Mol. Cell. Proteomics *11*, 202–214.

Seger, R., and Krebs, E.G. (1995). The MAPK signaling cascade. FASEB J. *9*, 726–735.

Shah, N.P., Tran, C., Lee, F.Y., Chen, P., Norris, D., and Sawyers, C.L. (2004). Overriding imatinib resistance with a novel ABL kinase inhibitor. Science *305*, 399–401.

Sos, M.L., Fischer, S., Ullrich, R., Peifer, M., Heuckmann, J.M., Koker, M., Heynck, S., Stückrath, I., Weiss, J., Fischer, F., et al. (2009). Identifying genotype-dependent efficacy of single and combined PI3K- and MAPK-pathway inhibition in cancer. Proc. Natl. Acad. Sci. USA *106*, 18351–18356.

Statsuk, A.V., Maly, D.J., Seeliger, M.A., Fabian, M.A., Biggs, W.H., 3rd, Lockhart, D.J., Zarrinkar, P.P., Kuriyan, J., and Shokat, K.M. (2008). Tuning a three-component reaction for trapping kinase substrate complexes. J. Am. Chem. Soc. *130*, 17568–17574.

Tanaka, M., Bateman, R., Rauh, D., Vaisberg, E., Ramachandani, S., Zhang, C., Hansen, K.C., Burlingame, A.L., Trautman, J.K., Shokat, K.M., and Adams, C.L. (2005). An unbiased cell morphology-based screen for new, biologically active small molecules. PLoS Biol. *3*, e128.

Wilson, T.R., Fridlyand, J., Yan, Y., Penuel, E., Burton, L., Chan, E., Peng, J., Lin, E., Wang, Y., Sosman, J., et al. (2012). Widespread potential for growth-factor-driven resistance to anticancer kinase inhibitors. Nature *487*, 505–509.

Zhu, Z., Aref, A.R., Cohoon, T.J., Barbie, T.U., Imamura, Y., Yang, S., Moody, S.E., Shen, R.R., Schinzel, A.C., Thai, T.C., et al. (2014). Inhibition of KRAS-driven tumorigenicity by interruption of an autocrine cytokine circuit. Cancer Discov. *4*, 452–465.